Uncovering Manifold Structures in Robonaut's Sensory-Data State Space

Richard Alan Peters II
Center for Intelligent Systems
Vanderbilt University School of Engineering
Nashville, TN 37235
Alan.Peters@Vanderbilt.Edu

Odest Chadwicke Jenkins
Department of Computer Science
Brown University
Providence, RI 02912-1910
cjenkins@cs.brown.edu

***Abstract*— This paper presents results from the application of dimensionality reduction algorithms to sensory-data time-series that were recorded from Robonaut – NASA's humanoid robot – while it was being teleoperated through three tool manipulation tasks. The algorithms tested were Principal Component Analysis, Multidimensional Scaling, and Spatio-Temporal Isomap. Structures were shown to exist in some cases, but their detection required careful analysis and a correct choice of parameters.**

I. Introduction

When a robot is programmed through demonstration or controlled through teleoperation, its resultant sensory-motor data stream can form discernable patterns in the vector space that contains them, the sensory-motor state space (SMSS). The patterns reflect both measurable effects on the environment of the robot's actions and its motor reactions to sensory input. Thus, the patterns emerge from a closed-loop interaction between robot and environment. The SMSS has dimension equal to the number of scalar signals that can be recorded while the robot operates. But, the effective dimension of the pattern may be much smaller, depending on the number of independent variables that dominate during the interaction. Dimensionality reduction algorithms can elucidate the structure of the patterns.

In cases of repetitive, constrained motion by the robot (for example repeatedly reaching toward and grasping an object) the dominant variables tend to trace closed manifolds in the SMSS. Closure makes sense because during exact repetitions of a task the trajectory through SMSS would repeat itself. If the task is repeated with some variations, say under different initial conditions in robot or environment, the trajectory does not repeat itself exactly. Instead, a family of trajectories lies on a closed surface in the SMSS, displaced from one another along directions that correspond to the variations. By having the robot perform the same task under different initial conditions, limits on the manifold might be discerned.

Knowledge of the SMSS manifolds that correspond to various tasks and scenarios would be valuable since it could lead to compact descriptions of fundamental behaviors (encapsulation or macro generation), real-time behavior interpolation, recognition of key events or unexpected events during task execution, recognition of intentionality in the perceived behavior of a collaborator (human or robot), or the generalization of related tasks through the detection of vector space homeomorphisms. Functional or numerical descriptions of these manifolds could also lead to solutions of the grounding problem.

A. The Grounding Problem

The symbol grounding problem is one of central importance to cognitive science and artificial intelligence [1]. That is, how does an abstract representation of the physical – an object, a process, or a phenomenon – come to be associated with its physical actuality? Philosophically, symbol grounding is related to the classical problem of meaning and, therefore, has been pondered in many forms for many years by many people [2]. In robotics, it is the problem of meeting objectives or sub-goals through sensing, actuation, and computation [3]. An analogy can be drawn to the neuro-ethological problem of understanding the neural correlates of the behavior of animals [4].

The coordination of sensing with action, or *Sensory-Motor Coordination* (SMC) is surely necessary for an animal to survive or for a robot to do anything useful. Pfeifer has shown that SMC data can self-organize into descriptors that categorize the robot-environment interaction [5]. He demonstrated that if $\mathbf{x}_k : \{1, 2, 3, \ldots N\} \rightarrow \mathbb{R}^n$ is a vector time series of SMC data recorded by a robot that is executing a fixed set of tasks in a simple but changing environment, then the set of vectors, $\{\mathbf{x}_k\}_{k=1}^{N}$ effectively forms clusters in $\mathbb{R}^n$. He argued that this self-organization of the data in effect described a categorization of the environment with respect to SMC. It follows that the SMSS locus of a cluster corresponds to a class of motor action taken under specific sensory conditions or, in duality, to a set of expected environmental responses to specific motor activity.

If SMC results in the formation of manifolds in the SMSS it can be argued that, in effect, SMC categorizes the physical world through the uncovering of the structure latent in robot-environment interaction. In doing so, it can further be argued that SMC provides a means to address the symbol grounding problem ... for robots at least.

This paper presents results from the application of dimensionality reduction algorithms, including spatio-temporal Isomap [6], to sensory-data time-series recorded during the teleoperation of Robonaut. The manifolds that correspond to three different tasks are described and discussed.

Fig. 1. Robonaut, NASA's space capable humanoid robot.

TABLE I

SIGNALS RECORDED FROM ROBONAUT.

Signal	Dimension
End-effector position, actual	3
End effector rotation mat, actual	9
Arm orbit angle, actual	1
End-effector position, requested	3
End effector rotation mat, req'd	9
Arm orbit angle, requested	3
Arm 3-axis force on wrist	3
Arm 3-axis torque on wrist	3
Arm 3-axis force on shoulder	3
Arm 3-axis torque on shoulder	3
Arm joint positions	7
Arm joint torques	7
Hand force on fingers	5
Hand joint positions	12
Hand joint torques	12
Hand tactile sensors	19
Visual object name	1
Visual object pose	6
Teleoperator voice command	1

II. PREVIOUS WORK

In [7] a single SMSS trajectory was learned over six trials that could later be performed autonomously with success in the face of small variations in the environment or perturbations of the goal. Later it was shown that sets of such learned trajectories could be interpolated to provide intermediate results [8]. In addition to Pfeifer [5], many others have studied the extraction of SMC parameters, including Cohen [9], Grupen [10], Lungarella [11], and Peters [12].

The use of motion data to plan robotic motion is a problem that has been studied by Matarić [13], Jenkins and Matarić [14], Ude et al. [15], Pollard et al. [16], and Atkeson et al. [17]. Matarić and Jenkins have enabled a simulated humanoid to learn unconstrained motion patterns from human motion-capture data. Jenkins has further studied the creation of new motions through the interpolation of learned trajectories using Isomap [18]. Isomap is one of a number of dimensionality reduction techniques including Principal Component Analysis and the related Singular Value Decomposition, both of which are textbook approaches, Multi-dimensional Scaling and Locally Linear Embedding [19]. Application of dimensionality reduction to robotics has been done by Asada [20] MacDorman [21], and others.

III. RESEARCH HARDWARE

Experiments were performed on Robonaut, NASA's space-capable, humanoid robot. (Fig. 1). Robonaut was developed by the Dexterous Robotics Laboratory of the Automation, Robotics, and Simulation Division of the NASA Engineering Directorate at Lyndon B. Johnson Space Center in Houston, Texas [22]. Each seven degree of freedom (DoF) Robonaut arm is approximately the size of a human arm. Each of those mates with a 12-DoF hand to produce a 19-DoF upper extremity. The robot has manual dexterity sufficient to perform a wide variety of tasks requiring the intricate manipulation of tools and other objects.

Robonaut's sensors include a color, stereo camera platform embedded in a head that is mounted on a 3-DoF neck, and binaural microphones located on opposite sides of the head, parallel to the stereo camera baseline. The two hand/wrist modules contain 84 sensors for feedback and control. Each DoF has a motor position sensor, a joint force sensor, and a joint absolute position sensor. The two arm modules contain 90 sensors. Each actuator contains a motor incremental position sensor, redundant joint torque sensors, redundant joint absolute position sensors, and four temperature sensors distributed throughout the joint. Each arm employs relative optical encoders in five of its joints. The encoders reside on the motor side of the gear train and have resolutions ranging between 200 and 1000 counts per degree of arm motion. (See [23] for a more detailed description of the Robonaut mechatronics.) The data signals that were recorded from Robonaut during teleoperation are listed in Table I. The resulting 110-dimensional vector time-series was recorded at a nominal rate of 50Hz.

Although Robonaut is physically capable of autonomous operation it is most often controlled directly via teleoperation wherein every motion made by Robonaut reflects a similar motion made by the operator, who perceives the robot's workspace through full-immersion virtual reality. The operator wears a helmet that enables him or her to see through the robot's stereo camera head and to hear through the robot's binaural microphones. Sensors in gloves worn by the operator determine Robonaut's finger positions. Six-axis Polhemus sensors [24] on the helmet and gloves determine the robot's arm and head positions. An operator guides the robot using only vision; there is neither direct haptic nor direct force feedback from robot to person.

IV. Methods and Procedures

One simple experiment using a computer mouse and three experiments using Robonaut in teleoperation were performed. The resulting data were analyzed using principal component analysis (PCA), multi-dimensional scaling (MDS), and spatio-temporal ISOmap (STI).

The first experiment contrasts the results of a standard Isomap analysis with a Spatio-Temporal Isomap analysis of data that has two spatial dimensions and one time dimension. Fig. 2 illustrates the data (drawn from blue to red with respect to time) collected from mouse movements. The data was generated by repeatedly moving the mouse up and down from two common points while expanding the contour in the middle to cover a crescent moon shape. Immediately after one crescent was formed the mouse was moved to another position on the plane and the process was repeated to create a second crescent. This data set provides a baseline with respect to simplicity.

A. Data Collection and Robonaut Teleoperation

As Robonaut operates, either autonomously or via teleoperation, it continually publishes its sensory and motor data at a nominal rate of 50 Hz. The 110 scalar signals (listed in Table I) were recorded during the experiments and later analyzed as a 110-dimensional vector time-series. The three experiments were:

1) Robonaut reached toward, and grasped a vertically oriented wrench five times at each of nine locations in its workspace.
2) Robonaut held a power drill rigged to be a socket driver, in such a way that it could actuate the trigger with its index finger. The robot was teleoperated to mate the socket to the four lug nuts on a wheel and then to actuate the trigger to rotate the socket. Four trials were deliberate failures and twenty (five each at each of the four lug nuts) were successful.
3) Robonaut reached for, grasped, and lifted the power drill out of a holster then verified that it was in the correct position to actuate the trigger. This was repeated four times.

For experiment 1, five of the teleoperated grasps were analyzed. In the other two experiments, all the trials we analyzed. PCA, MDS, and STI were used. The analysis presented here focused entirely on the sensor subspace of the SMSS. The reason was that Jenkins had previously found clearly discernible manifolds in the motor/position data vector space derived from human motion capture data [25]. Similar manifolds were found in the Robonaut motor subspace data. The 3-D motion in space dominates the sensory vectors (when they are weighted equally) to such an extent that the sensory effects are not detectable via dimensionality reduction. Therefore, the sensor subspace was analyzed in isolation. The 30 motor data signals, including motor actuation forces and joint position and velocity, were zeroed out. The remaining 80 variables contained sensory data, comprising tactile sensors on the fingers and force sensors at various places on the robot. All the variables were normalized to a common range.

B. Uncovering Manifolds with Spatio-temporal Isomap

Spatio-temporal Isomap [6] was used to uncover manifolds underlying sensory data from Robonaut teleoperation. (This, of course, presupposes that the manifolds are *spatio-temporal manifolds* and can be uncovered by ST-Isomap.) A spatio-temporal manifold, an example of which is shown in Fig. 2 can be described structurally as a $1+\epsilon$-manifold curve in an embedding space. Successive locations on it represent successive time-instants in the spatio-temporal process. Each location on the curve also encapsulates all of the spatial variations representing a certain fixed spatio-temporal progress. Thus, a diverse set of spatial variations that correspond to the same spatio-temporal progress is collapsed into a single location in the embedded manifold.

Assume input data are samples from a continuous process. Then the general procedure for ST-Isomap is:

1) window the input data into temporal blocks S;
2) compute a sparse L_2 distance matrix D^l from local neighborhoods $\texttt{nbhd}(S_i)$ about each point S_i;
3) locally identify the *common temporal neighbors* $\texttt{CTN}(S_i)$ of each point S_i as the *K-nearest nontrivial neighbors* $\textit{KNTN}()$;
4) reduce distances in $D^l_{S_i,S_j}$ between points with common and adjacent temporal relationships such that

$$D^0_{S_i,S_j} = \begin{cases} D^l_{S_i,S_j}/(c_{\text{CTN}}c_{\text{ATN}}) & \text{if } S_j \in \texttt{CTN}(S_i) \\ & \text{and } j = i+1 \\ D^l_{S_i,S_j}/c_{\text{CTN}} & \text{if } S_j \in \texttt{CTN}(S_i) \\ D^l_{S_i,S_j}/c_{\text{ATN}} & \text{if } j = i+1 \\ \texttt{penalty}(S_i,S_j) & \text{otherwise} \end{cases} \quad (1)$$

5) complete D^0 into a full all-pairs shortest-path distance matrix, $D = D^g$ (via Dijkstra's algorithm), such that $g \geq |S|$:

$$D^g_{i,j} = \begin{cases} D^0_{i,j} & g = 0 \\ \texttt{min}(D^{g-1}_{i,j}, D^{g-1}_{i,k} + D^{g-1}_{k,j}) & g \geq 1 \end{cases} \quad (2)$$

6) embed D into d_e-dimensional embedding space through MDS such that:

$$E = |D^g - D_e|_{L^2} \quad (3)$$

where `nbhd()` are the local neighbors of given segment, c_{CTN} and c_{ATN} are constants for increasing similarity between common and adjacent temporal neighbors, D_e is the matrix of Euclidean distances in the embedding, and $\|A\|$ is the L^2 matrix norm of A. $\texttt{penalty}(S_i,S_j)$ is a function that determines the distance between a pair with no temporal relationship, typically set as $D^l_{S_i,S_j}$.

STI differs from simply adding a notion of velocity into the data. Velocity alone provides only for *proximal disambiguation* of spatially proximal yet structurally different data points in the input space. In addition to proximal disambiguation, STI can find the *distal correspondence* of spatially distal data points in the input space that share common spatio-temporal structure. Such correspondences are performed through the application of Dijkstra's algorithm which enforces *transitivity* between a data pairs with a CTN relationship.

V. Results and Discussion

The mouse-movent experiment is illustrated in Fig. 2. In 3-D spacetime, the trajectory on a single crescent would zig-zag between the two endpoints while increasing in displacement from the line segment connecting them (a). Since standard Isomap does not treat time as any different from space, the embedding (b) looks very similar to the original spatial plot (a). Both temporally windowed MDS and STI, however, account for the temporal adjacency of points and, therefore, discern a cyclic process. The resulting continuous embeddings (with KNTN = 3), have two loops connected by a transition. STI favors the temporal similarity of the repetitions over the spatial divergence to produce a family of closely spaced loops (e). In fact, these collapse into a single loop (f) as the common temporal neighbors (CTN) are lumped. (g) more clearly shows the procedural connectivity (*i.e.*, the similarity of points with respect to temporal evolution the process) of the CTN.

The STI embedding of the wrench experiment sensory data is shown in Figure 3 with a comparison to embedding by PCA. The structure of the grasps can be surmised from the PCA embedding, (a) and (b), but it does not clearly identify the procedural similarities in the trials. In contrast, the common procedural structure of the task trials is apparent in the STI embedding, (c)-(e). There are five contours that more or less parallel each other. Each represents the sensory response of a single task trial. These appear to trace a clear sensory manifold made up of four (perhaps five) sub-manifolds. Each sub-manifold corresponds to a specific behavior in the task. The black points mark the start of each trial. The green curves (on the right lobe of the "bow-tie" structure in (c) and (d) and on the left in (e)) represent the reach toward the wrench. The red lines (that connect the two lobes of the bow through a short distance) represent the closure of the grasp on the wrench. The cyan contours that make up the bulk of the other lobe indicate the holding of the wrench. The long magenta curves (that connect the lobes through a longer distance) represent the grasp release. The yellow contours (that are intermingled with the green ones) correspond to the retraction of the arm from the wrench.

The structure uncovered from the reach and grasp data appears to characterize the sensor values at different episodes during the task. If that were actually so, then the model would describe the evolution of the sensory response to another instance of the task (that was not used in the original analysis). Given sensory data for this new trial, the training grasps, and the embedded training grasps, interpolation can be used to map the new sensory-data time-series onto the structure found in the embedding space. Shepard's interpolation was used here to perform the mapping. The result is shown in Figure 3 (g) and (h). It would appear to demonstrate a faithful uncovering of a spatio-temporal manifold in sensor data.

While STI performed well with the grasp data, it yielded mixed results with respect to the drill mating and holster grasp data sets. The manifolds estimated by STI for those data do not produce as clear a mapping of the sensory data. An appropriately extracted looping structure can be seen in the STI embedding. However, this result required a significant amount of parameter tuning. We believe the artifacts in the STI embedding are the result of estimating *hard* spatio-temporal correspondences between common temporal neighbors. Such hard decisions make selecting a specific setting for neighborhood size a difficult, if not impossible, task. We are currently exploring methods to incorporate soft decisions in spatio-temporal neighborhood determination.

To avoid hard spatio-temporal correspondences, we focused on proximal disambiguation in sensor data by using multidimensional scaling on temporal windows of sensor data. This windowed MDS enables us to visualize a sensory space similar to PCA. Windowed MDS is essentially PCA on windowed data; however, MDS is tractable for high-dimensional datasets, unlike PCA. Windowed MDS on the drill mating data successfully uncovered the basic looping structure of the mating task. Furthermore, the pressure applied during the mating of the drill and the nut is accurately disambiguated in the embedding. In the holster grasping task, none of the dimension reduction techniques appeared to uncover meaningful structure. We attributed the difficulty in analyzing this dataset to the amount of data being overly sparse for the amount of variation contained in the data.

VI. Conclusion

Our analysis of the sensory data from Robonaut yielded excellent structural results in one of the three cases analyzed. In a second case some structure was discernible but only with a highly tuned parameter set. The third case yielded no discernably useful structuring information. Our results were limited, moreover, by the fact that we analyzed sensory data apart from the corresponding motor components. True detection of the manifolds that describe SMC will require the analysis of the coupled data. Such work continues.

Acknowledgements

This work was funded in part by NASA grants NAG9-1446, NAG9-1515, and NNJ04HI19G.

References

[1] S. Harnad, "The symbol grounding problem," *Physica D*, vol. 42, pp. 335–346, 1990.

[2] A. T. Peperzak, *The Quest for Meaning: Friends of Wisdom From Plato to Levinas*. Fordham University Press, 2003.

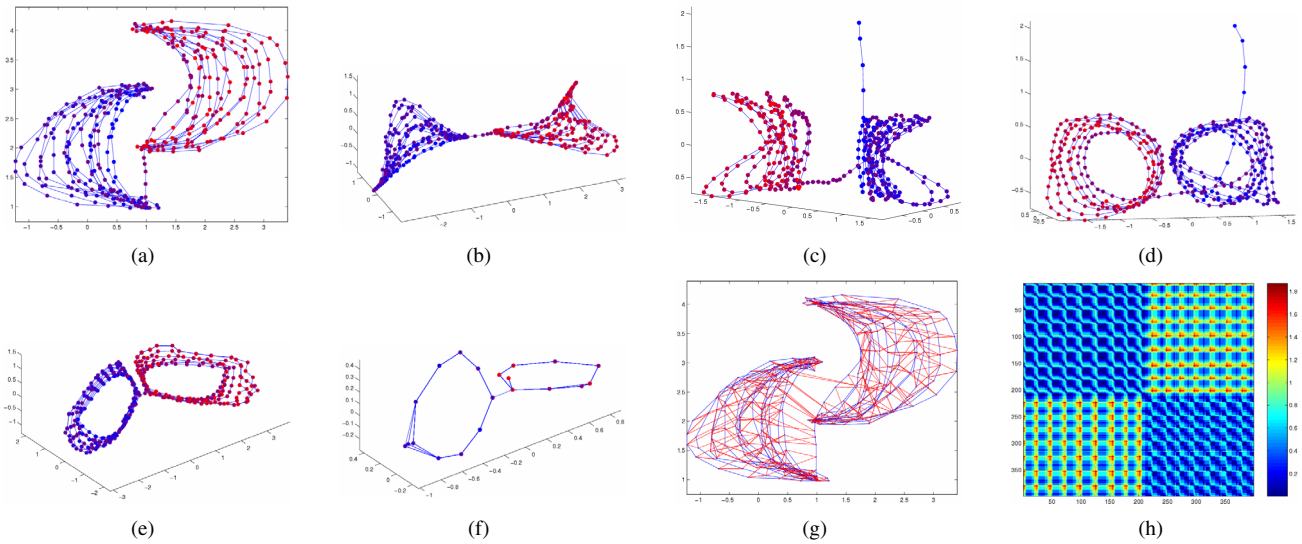

Fig. 2. (a) A 2D mouse-click trajectory color coded from blue to red to indicate progress through time. (b) Embedding of the trajectory using standard (non-ST) Isomap. (c,d) Two views of the trajectory embedded by temporally-windowed MDS. (e,f) Two STI embeddings of the trajectory showing a collapse of the trajectories that results from higher c_{ctn} values. (g,h) The spatio-temporal correspondences and the spatio-temporal distance matrix computed by STI.

[3] L. Floridi, "Open problems in the philosophy of information," *Metaphilosophy*, vol. 35, no. 4, pp. 554–582, 2004.

[4] R. Kortmann, "Embodied cognitive science," in *Proceedings Of Robo Sapiens - The First Dutch Symposium On Embodied Intelligence* (W. de Back, T. van der Zant, and L. Zwanepol, eds.), vol. 24 of *Artificial intelligence preprint series*, Universiteit Utrecht, 2001.

[5] R. Pfeifer and C. Scheier, *Understanding Intelligence*. The MIT Press, Cambridge, MA, 1999.

[6] O. C. Jenkins and M. J. Matarić, "A spatio-temporal extension to isomap nonlinear dimension reduction," in *The International Conference on Machine Learning (ICML 2004)*, (Banff, Alberta, Canada), pp. 441–448, July 2004.

[7] R. A. Peters II, C. L. Campbell, W. J. Bluethmann, and E. Huber, "Robonaut task learning through teleoperation," in *Proceedings of the 2003 IEEE International Conference on Robots and Automation*, (Taipei, Taiwan), Oct. 2003.

[8] C. L. Campbell, R. A. Peters II, R. E. Bodenheimer, W. J. Bluethmann, E. Huber, and R. O. Ambrose, "Superpositioning of behaviors learned through teleoperation," *IEEE Transactions on Robotics*, vol. to appear, 2006.

[9] P. R. Cohen and N. Adams, "An algorithm for segmenting categorical time series into meaningful episodes," in *Proceedings of the Fourth Symposium on Intelligent Data Analysis*, vol. 2189, pp. 198–207, 2001.

[10] J. A. Coelho Jr., J. H. Piater, and R. A. Grupen, "Developing haptic and visual perceptual categories for reaching and grasping with a humanoid robot," in *Proceedings of the First IEEE/RAS International conference on Humanoid Robots (Humanoids 2000)*, Sept. 2000.

[11] M. Lungarella, T. Pegors, D. Bulwinkle, and O. Sporns, "Methods for quantifying the information structure of sensory and motor data," *Neuroinformatics*, vol. 3, pp. 243–262, Fall 2005.

[12] M. E. Cambron and R. A. Peters II, "Determination of sensory motor coordination parameters for a robot via teleoperation," in *Proceedings of the 2001 IEEE International Conference on Systems, Man, and Cybernetics*, vol. 5, pp. 3252–3257, Oct. 2001.

[13] M. J. Matarić, "Getting humanoids to move and imitate," *IEEE Intelligent Systems*, vol. 15, pp. 18–24, July 2000.

[14] O. C. Jenkins and M. J. Matarić, "Performance-derived behavior vocabularies: data-driven acqusition of skills from motion," *International Journal of Humanoid Robotics*, vol. 1, pp. 237–288, June 2004.

[15] A. Ude, C. G. Atkeson, and M. J. Riley, "Planning of joint trajectories for humanoid robots using b-spline wavelets," in *Proceedings of the IEEE International Conference on Robotics and Automation*, pp. 2223–2228, Apr. 2000.

[16] N. S. Pollard, J. K. Hodgins, M. J. Riley, and C. G. Atkeson, "Adapting human motion for the control of a humanoid robot," in *Proceedings of the 2002 IEEE International Conference on Robotics and Automation*, pp. 1390 – 1397, May 2002.

[17] C. G. Atkeson, J. G. Hale, F. Pollick, M. J. Riley, S. Kotosaka, S. Schaal, T. Shibata, G. Tevatia, A. Ude, S. Vijayakumar, and M. Kawato, "Using humanoid robots to study human behavior," *IEEE Intelligent Systems*, vol. 15, pp. 46–56, July 2000.

[18] J. B. Tenenbaum, V. de Silva, and J. C. Langford, "A global geometric framework for nonlinear dimensionality reduction," *Science*, vol. 290, pp. 2319–2323, 22 December 2000.

[19] S. Roweis and L. Saul, "Nonlinear dimensionality reduction by locally linear embedding," *Science*, vol. 290, pp. 2323–2326, Dec. 2000.

[20] M. Asada, M. Ogino, S. Matsuyama, and J. Ooga, "Imitation learning based on visuo-somatic mapping," in *Proceedings of 9th International Symposium on Experimental Robotics*, vol. CD-ROM, (Singapore), Springer-Verlag, June 2004.

[21] K. F. MacDorman, R. Chalodhorn, and M. Asada, "Periodic nonlinear principal component neural networks for humanoid motion segmentation, generalization, and generation," in *Proceedings of the Seventeenth International Conference on Pattern Recognition*, (Cambridge, UK), pp. 537–540, International Association for Pattern Recognition, Aug. 2004.

[22] R. O. Ambrose, H. Aldridge, R. S. Askew, R. R. Burridge, W. Bluethmann, M. Diftler, C. Lovchik, D. Magruder, and F. Rehnmark, "Robonaut: Nasa's space humanoid," *IEEE Intelligent Systems*, vol. 15, pp. 57–63, July 2000.

[23] Robonaut Development Team, "Robonaut avionics," tech. rep., NASA Johnson Space Center, http://robonaut.jsc.nasa.gov/Avionics.htm, July 2004.

[24] J. C. Krieg, "Motion tracking: polhemus technology," *Virtual Reality Systems*, vol. 1, pp. 32–36, Mar. 1993.

[25] O. C. Jenkins, *Data-driven Derivation of Skills for Autonomous Humanoid Agents*. PhD thesis, University of Southern California, Robotics Research Laboratory, Center for Robotics and Embedded Systems, Computer Science Department, University of Southern California, 941 W. 37th Place, Los Angeles, CA 90089 USA, 2003.

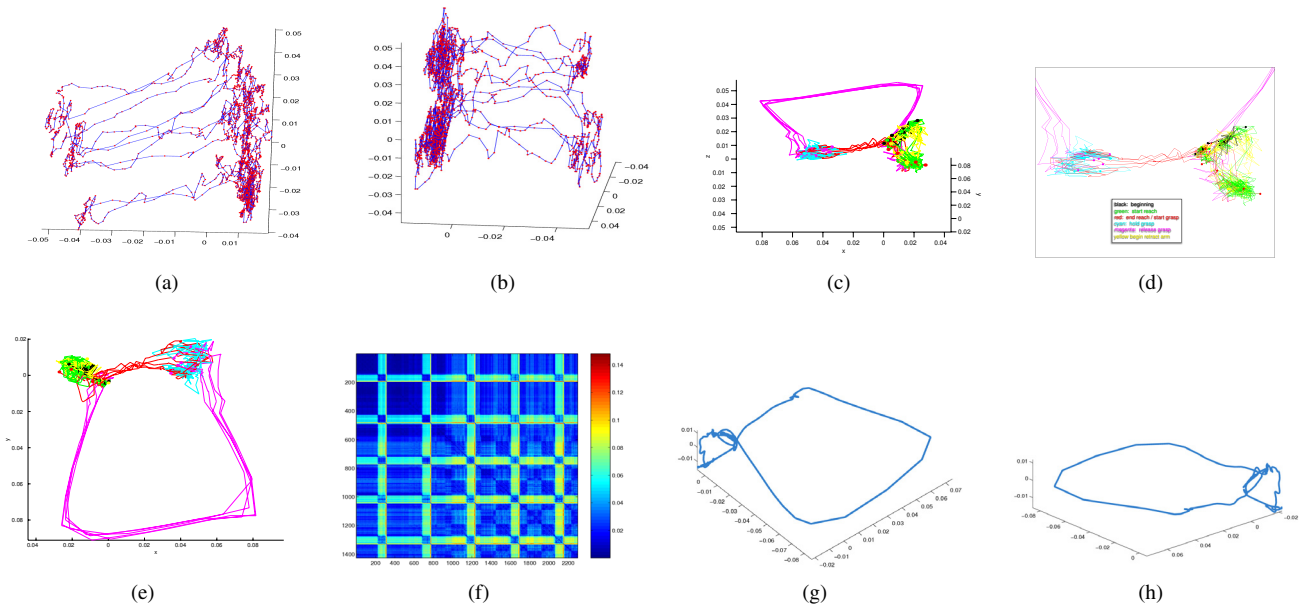

(a) (b) (c) (d)

(e) (f) (g) (h)

Fig. 3. (a,b) Two views of the PCA embedding for the grasp data from Robonaut teleoperation. (c,d) Two views of the same data embedded by sequentially continuous STI. (f) Distance matrix for the STI embedding. (g,h) A test grasp mapped via Shepards interpolation onto the grasp structure in the STI embedding.

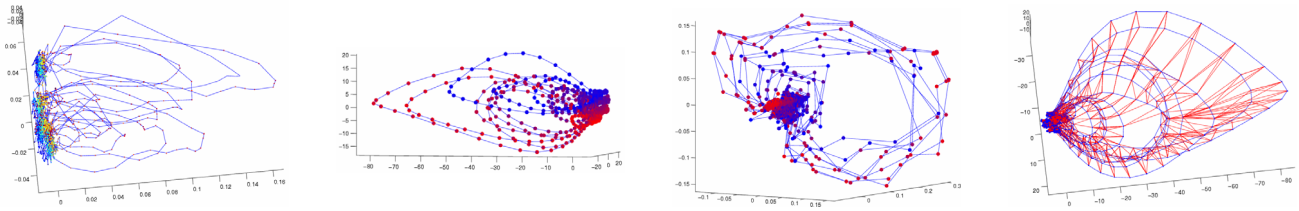

(a) (b) (c) (d)

Fig. 4. Embedding of the drill-to-nut mating sensor data with (a) PCA, (b) temporally-windowed MDS, and (c) STI. (d) Spatio-temporal correspondences computed by STI.

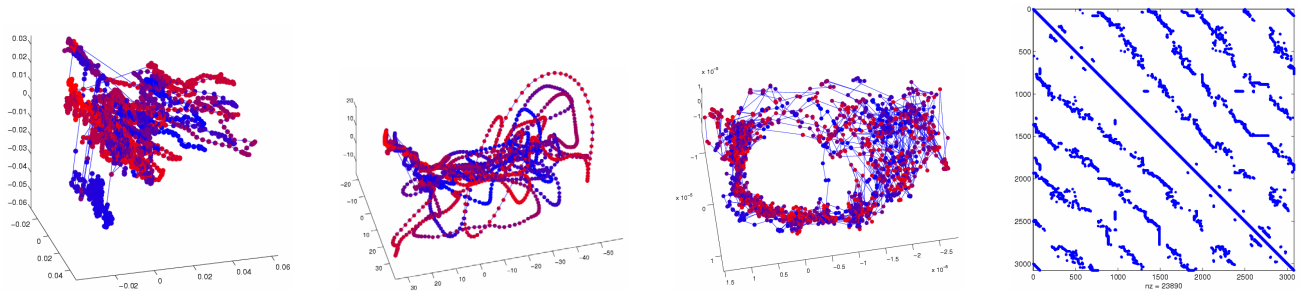

(a) (b) (c) (d)

Fig. 5. Embedding of the take-drill-out-of-holster task sensor data using (a) PCA, (b) temporally-windowed MDS, and (c) STI. (d) Spatio-temporal connectivity matrix computed by STI.